Research Square

Preprints are preliminary reports that have not undergone peer review.
They should not be considered conclusive, used to inform clinical practice,
or referenced by the media as validated information.

Quantitative digital pathology reveals reversal of MASH-related liver damage following bariatric surgery

Alina Onoiu

alinaiuliana.onoiu@iispv.cat

Hospital Universitari Sant Joan de Reus https://orcid.org/0009-0006-9483-498X

Lara Murray

Ylaine Gerardin

Geetika Singh

Robert Egger

PathAI

Sergio González-Serrano

Vicente Cambra-Cortés

https://orcid.org/0009-0002-9574-6261

Andrea Jiménez-Franco

https://orcid.org/0000-0002-4251-585X

Carmen Guilarte

David Parada

Jordi Camps

Jorge Joven

Article

Keywords: Digital Imaging, Immune System, MASH Remission, Laparoscopic Sleeve Gastrectomy, Liver Zonation

Posted Date: February 27th, 2026

DOI: https://doi.org/10.21203/rs.3.rs-8725050/v1

License: This work is licensed under a Creative Commons Attribution 4.0 International License.
Read Full License

Additional Declarations: There is **NO** Competing Interest.

Abstract

Metabolic dysfunction-associated steatohepatitis (MASH) is a progressive liver disease characterized by steatosis, inflammation, hepatocellular injury, and fibrosis that may progress to cirrhosis or hepatocellular carcinoma. While laparoscopic sleeve gastrectomy (LSG) effectively treats severe obesity and improves liver histology, traditional pathological assessments rely on subjective evaluations. This study aimed to objectively assess LSG impact on MASH histological outcomes using digital pathology.

We conducted a retrospective study analyzing paired liver biopsies from 44 patients who required a second bariatric intervention due to suboptimal outcomes following initial LSG. Wedge biopsies were obtained during both surgical procedures using standardized techniques, allowing comparisons between specimens obtained at the initial intervention and post-LSG. The liver tissue sections were digitized and analyzed using LiverExplore, an artificial intelligence (AI)-powered digital pathology tool to quantify hepatic cellular features, tissue architecture, and collagen characteristics.

LSG resulted in significant improvements in key histopathological parameters, including reduced hepatic steatosis ($p = 7.2\times10^{-9}$) and hepatocellular ballooning ($p = 2.6\times10^{-4}$). While overall fibrosis scores remained unchanged, distinct fibrotic subtypes demonstrated marked improvement, with significant reductions in periportal fibrosis ($p = 2.2\times10^{-4}$), incomplete septal fibrosis ($p = 6.9\times10^{-6}$), and complete septal fibrosis ($p = 6.6\times10^{-4}$). The hepatic immune landscape showed comprehensive reorganization with increased neutrophil ($p = 6.4\times10^{-5}$) and eosinophil ($p = 5.3\times10^{-4}$) infiltration, alongside zonal redistribution of immune cells throughout the liver parenchyma.

AI-enhanced digital pathology enables objective assessment of hepatic changes post-bariatric surgery. LSG improved key MASH features. Post-surgical increase in neutrophils and eosinophils along with zonal immune reorganization suggests immune-mediated tissue remodeling contributing to recovery. These findings support LSG efficacy for MASH treatment and demonstrate AI utility in capturing complex pathological changes.

Introduction

Obesity is a complex and progressive chronic disease that has a growing negative impact on healthcare. In the United States, over 10% of individuals with obesity meet the criteria for severe obesity, which is defined as having a body mass index (BMI) of 40 kg/m² or higher[1,2]. This condition is associated with a higher risk of mortality due to a greater incidence of comorbidities such as cardiovascular disease, cancer, liver disease, and other life-threatening metabolic complications[3,4]. Effectively managing severe obesity requires a deeper understanding of the risks and mechanisms related to weight-associated diseases. One specific condition, metabolic dysfunction-associated steatotic liver disease (MASLD), is common among these patients and can progress to metabolic dysfunction-associated steatohepatitis (MASH), fibrosis, cirrhosis, and hepatocellular carcinoma[5,6]. The urgent need for timely diagnosis and intervention for patients with MASH highlights the importance of weight management strategies [7–9].

Significant weight loss in cases of severe obesity through well-designed, structured, and comprehensive lifestyle intervention programs is often anecdotal. Several medications are now available for the long-term treatment of obesity, including semaglutide, a glucagon-like peptide 1 (GLP-1) agonist. Notably, patients treated with semaglutide lose an average of 6% to 12% of their initial body weight, with demonstrated liver histology improvement in patients with MASH, leading to its recent FDA approval for this indication[10–12]. Bariatric procedures can also be effective for weight loss; however, these strategies have potential drawbacks including surgical risks, perioperative complications, nutritional deficiencies, the need for lifelong dietary modifications, and variable long-term weight regain[13]. The most commonly performed bariatric surgeries are laparoscopic sleeve gastrectomy (LSG), which accounts for 60.4% of procedures, and Roux-en-Y gastric bypass, which makes up 25.5% of procedures, and aim for target weight losses of 25% to 30% and 30% to 35%, respectively[14]. Such losses do not permanently resolve obesity but can be effective for managing MASH[6–9,15,16]. Demonstrating long-term efficacy of these interventions remains challenging, and real-world data indicate that weight loss alone does not result in MASH improvement[17]. Recently resmetirom was approved for the treatment of F2/F3 MASH, and weight loss was negligible, while semaglutide has also been approved for the same condition and provides additional metabolic effects[18,19].

While less invasive alternatives to biopsies for disease monitoring have been investigated, histological assessment of liver tissue remains the gold-standard[20]. Regulatory approvals for new therapeutics necessitate demonstrating MASH resolution without worsening fibrosis and improving fibrosis without worsening MASH[21] Artificial intelligence (AI) algorithms have enabled granular characterization of liver histology in MASH and other liver diseases[22,23]. As the field of pathology transitions to a more digital workflow, the integration of AI algorithms to assist pathologists with diagnosis and other tasks is becoming a reality[24–27].

In this study, we employed AI pathology tools to evaluate a clinically significant yet understudied cohort: patients with severe obesity and liver injury, before and after LSG[28]. By employing comprehensive histological assessment tools, we provide novel insights into the long-term hepatic outcomes of LSG, addressing a critical knowledge gap in this complex patient population.

Materials and Methods

Study Design and Participants

This retrospective, longitudinal, observational study was conducted in accordance with the Declaration of Helsinki and received ethical approval from the Institutional Review Board (PL4NASH112/2021, and EOM 244/2024). The included participants represent a subset of a broader prospective cohort enrolled in an ongoing study registered at ClinicalTrials.gov (Clinical Trial Number: NCT05554224 || https://clinicaltrials.gov/study/NCT05554224; registration date: 2022/09/21). All participants provided written informed consent prior to enrollment.

Paired liver biopsy samples were obtained during a primary LSG and a subsequent revisional bariatric surgery from 44 patients who required a revisional bariatric surgery due to insufficient weight loss or weight regain at Hospital Universitari Sant Joan in Reus, Spain.

At the time of the first intervention, all included patients were over 18 years old, had a BMI of 40 kg/m² or higher and presented high-risk comorbidities, such as a diagnosis or treatment for hypertension, dyslipidemia, or type 2 diabetes mellitus. All patients had received positive psychiatric evaluations for bariatric surgery. Patients with clinical or laboratory evidence of chronic or acute inflammation, infectious diseases, severe illness, hepatitis diagnosis or current cancer were excluded.

Sampling and histological procedures

Hepatic wedge biopsies were obtained intraoperatively under direct visualization by the same surgical team from the same liver segment in all patients to ensure anatomical consistency[29]. Following extraction, tissue sections were immediately formalin-fixed, paraffin-embedded, and sectioned at 4 μm thickness for histologic evaluation. Routine staining included hematoxylin and eosin (H&E) and Masson trichrome (MT) for assessment of steatosis, hepatocellular ballooning, lobular inflammation, and fibrosis.

Additionally, immunohistochemistry (IHC) was performed using the fully automated Ventana BenchMark ULTRA system (Roche Diagnostics Corporation, Indianapolis, IN, USA) in combination with the OptiView DAB IHC Detection Kit (Roche, Spain). To detect neutrophils, a specific primary antibody against CD15 was used (CONFIRM anti-CD15 [MMA], mouse monoclonal, Roche, Ref: 760–2504). Briefly, following automated antigen retrieval, tissue sections were incubated with the primary antibody, and immunoreactivity was visualized using DAB chromogen with hematoxylin counterstaining. Appropriate positive and negative controls were included in each staining batch to ensure specificity and reproducibility of the results.

An expert liver pathologist evaluated all samples using Nonalcoholic Steatohepatitis Clinical Research Network (NASH CRN) scoring parameters[20]. To minimize potential scoring bias, the pathologist performed blinded assessments without knowledge of sample timing or clinical data. The NAFLD Activity Score (NAS) was calculated by summing scores for steatosis, hepatocellular ballooning, and lobular inflammation. Patients were classified based on their NAS as follows: those with scores of 2 or lower were categorized as non-MASH (n = 1 at the first intervention and n = 27 at the second intervention), those with scores of 3 or 4 were classified as uncertain MASH (n = 4 at the first intervention and n = 10 at the second intervention), and those with scores of 5 or higher were classified as MASH (n = 39 at the first intervention and n = 7 at the second intervention).

Following initial evaluation, slides were digitized using a Ventana DP 200 scanner (Roche, Basel, Switzerland) at 40x magnification. H&E and MT-stained slides were analyzed using LiverExplore[30]

(PathAI, Boston, MA; For Research Use Only. Not for use in diagnostic procedures), while IHC slides were processed using the open-source software QuPath.

This study adhered to Good Clinical Practice guidelines and the Declaration of Helsinki, with Institutional Review Board approval under reference number EOMPI2024[244/2024]. Written informed consent was obtained from all participants.

Digital image analysis

LiverExplore

Histologic features of the liver microarchitecture were quantified using LiverExplore[30], a suite of algorithms that segment and classify tissue regions, lobular zones, cell types, and fibrosis subtypes from an H&E-stained whole slide image (WSI). Briefly, regions of lobular inflammation, hepatocellular ballooning, steatosis, portal inflammation, interface hepatitis, and normal hepatocytes are detected by the tissue model, as are tissue regions relevant to liver function (bile ducts and blood vessels). The cell model exhaustively classifies all nuclei in a WSI as one of eleven cell classes, including immune and inflammatory cells (e.g., neutrophils). Portal tracts, central veins, and surrounding lobular zones (zones 1, 2, and 3) are identified by the zonal model. Finally, all collagen is identified and classified as either non-pathological collagen or fibrosis subtypes corresponding to liver disease severity (e.g., complete septal fibrosis). All model outputs are visible as heatmap overlays and quantified as human interpretable features (HIF)[30,31].

IHC Signal Quantitation

IHC-stained slides were analyzed using QuPath (version 0.5.1), an open-source software for digital pathology analysis. Whole tissue sections were manually annotated as regions of interest (ROIs), and artifacts were excluded through careful visual inspection. Following ROI selection, the Positive Cell Detection tool was applied using a single intensity threshold to identify and classify $CD15^{+}$ and $CD15^{-}$ cells. After cell detection, quantitative data for each slide was exported for further analysis. Full methodological details, including parameter settings and thresholds used, are provided in the Supplementary Materials.

Statistical analyses

All statistical analyses were performed using RStudio (version 2024.09.0.375) and R (version 4.4.2). The dataset was complete with no missing values for any analyzed variables. Continuous variables were described using medians and interquartile ranges (IQRs), while categorical variables were reported as counts and percentages. Because most variables did not satisfy the assumptions of normality, non-parametric statistical methods were employed for comparisons.

Specifically, the Wilcoxon signed-rank test was used for comparisons involving continuous variables between two groups. For categorical data, the Chi-Squared test was utilized. To account for multiple comparisons across all HIFs, false discovery rate (FDR) correction was applied using Benjamini-Hochberg method. Statistical significance was set at ≤ 0.05.

Data visualization and graphical outputs were created in R and subsequently refined using Inkscape software (version 1.4.2) to enhance visual presentation quality.

Tomore specifically assess changes inthe relative areas of predicted fibrosis subtypes between interventions, a steatosis adjustment factor was implemented. This adjustment wasutilized to measure changes in fibrosis independent of LSG-induced reductions in steatosis. To calculate theadjusted fibrosis proportions, the area of each fibrosis subtype was divided by the difference between total tissue area and steatosis area *(*i.e., *Fibrosis Subtype Area / [Total Tissue Area - Steatosis Area]).*The underlying assumption of this approach is that any space taken up by steatosis is completely resolved and is not replaced by non-fibrotic liver tissue.

Results

1. Participants

Table 1 presents the selected demographic and clinical characteristics of the studied patients at both intervention time points. The cohort predominantly consisted of female participants, with a median interval of 5 years (IQR: 4-8 years) between interventions. BMI decreased significantly over this period, with a median reduction of 11.8 kg/m² (IQR: 10.2-14.7 kg/m2; *p*-value = $1.0x10^{-11}$).

Manual histopathological assessment by an expert liver pathologist revealed significant improvements in liver damage parameters between the two time points. Steatosis severity was notably higher in the first intervention group, with a greater proportion of participants in the two highest steatosis grades (>33% and >66%) compared to the second intervention time point (*p*-value = 1.0×10^{-6}). Similarly, hepatocellular ballooning was significantly reduced at the second intervention (*p*-value = 1.5×10^{-5}), with a higher number of participants exhibiting none or few ballooned hepatocytes.

Manual fibrosis staging demonstrated notable changes between interventions (*p*-value = 0.003). At the first intervention, the plurality (50%) of patients were at stage F3, characterized by bridging fibrosis, whereas at the second intervention, 59.1% of patients were at stage F2, characterized by perisinusoidal and periportal fibrosis. Lobular inflammation levels remained comparable between groups (*p*-value = 0.864).

The frequency of MASH decreased significantly between the first and second intervention (*p*-value = 2.2×10^{-6}). Supplementary Figure S1 illustrates the proportional distribution of participants diagnosed with MASH, non-MASH, and uncertain MASH status across both intervention time points.

Table 1. Main characteristics of included patients.

	1st Intervention	2nd Intervention	*p*-value
Women, n(%)	36 (81.8%)	36 (81.8%)	N/A
Age, years	44 [39 - 49]	49 [43 - 57]	$5.6x10^{-8}$
BMI, kg/m^2	52.4 [47.2 - 57.7]	40.6 [37.0 - 43.0]	$1.0x10^{-11}$
Liver Histologic Features			
Steatosis grade, n(%)			
< 5%	7 (15.9)	35 (79.5)	
5 – 33%	19 (43.2)	9 (20.5)	
> 33 – 66%	13 (29.5)	0	
> 66%	5 (11.4)	0	$1.0x10^{-6}$
Hepatocellular Ballooning, n(%)			
None	2 (4.5)	21 (47.7)	
Few cells	11 (25.0)	13 (29.5)	
Many cells	31 (70.5)	10 (22.7)	$1.5x10^{-5}$
Lobular inflammation, n(%)			
No foci	0	0	
< 2 foci	1 (2.3)	3 (6.8)	
2 – 4 foci	24 (54.5)	21 (47.7)	
> 4 foci	19 (43.2)	20 (45.5)	0.864
Fibrosis, n(%)			
None (F0)	0	0	
Perisinusoidal or periportal (F1)	0	4 (9.1)	
Perisinusoidal and periportal (F2)	21 (47.7)	26 (59.1)	
Bridging fibrosis (F3)	22 (50.0)	13 (29.5)	
Cirrhosis (F4)	1 (2.3)	1 (2.3)	0.003

2. Bariatric Surgery Induces Significant Changes in Hepatic Cellular Composition

LiverExplore enabled precise quantification of cellular composition changes within the hepatic parenchyma (Figure 1a). Results showed that LSG led to substantial alterations in hepatic cellular distribution (Figure 1b).

The proportion of total cells classified as normal hepatocytes increased significantly after LSG, rising from 39% to 48% of the total cells (*p*-value = 0.031; Figure 1c), suggesting a positive restoration of liver parenchyma. Additionally, there was a significant reduction in the fraction of steatotic hepatocytes, which decreased from 6.7% to 0.3%, with a *p*-value of $7.2x10^{-9}$ (Figure 1d). As depicted in Supplementary Figure S2, zonal analysis revealed that this improvement was most pronounced in Zone 3 ($p = 1.4\times10^{-7}$), where the proportion of steatotic hepatocytes was higher at the baseline, followed by Zone 2 ($p = 5.9\times10^{-8}$) and Zone 1 ($p = 9.3\times10^{-6}$), with post-intervention steatosis levels becoming uniform across all hepatic zones.

Similarly, ballooned hepatocytes, typically associated with advanced liver damage[32], declined from $2.53x10^{-4}$% to 0% of the total cells within evaluated tissue (*p*-value = $2.6x10^{-4}$; Figure 1e). Zone-specific analysis of ballooning showed significant reduction in Zone 2 (p = 0.011), while Zone 1 and Zone 3 did not reach statistical significance with a p-value of 0.090 and 0.052, respectively (Supplementary Figure S2). This reduction indicates that the bariatric surgery not only alleviates fatty infiltration but also reverses more severe forms of liver cell injury, contributing to a healthier liver phenotype. A comprehensive list of changes in cell features is found in Supplementary Table 1.

Unexpectedly, the first bariatric surgery led to an increase in the proportion of immune cells, rising from a median proportion of 27% to 31% of the total cells (*p*-value = 0.005; Figure 1f). This change suggests that the immune system may play a key role in the ongoing tissue remodelling process following the initial phase of weight loss, highlighting the complex interplay between inflammation and recovery in the liver.

3. Hepatic Immune System Reorganization Following Bariatric Surgery: The Central Role of Polymorphonuclear Cells

To characterize the observed increase in total immune cells post-intervention, we conducted a comprehensive analysis of immune cell subpopulations within the hepatic microenvironment. Significant compositional changes in the liver's immune landscape following surgery were detected (Figure 2a).

Prior to surgery, lymphocytes represented the predominant immune cell population, followed in descending order by macrophages, neutrophils, plasma cells, and eosinophils. Following surgery, while lymphocytes maintained their position as the most abundant immune cell type, a notable reorganization occurred with neutrophils emerging as the second most prevalent population, displacing macrophages to third position, followed by plasma cells and eosinophils.

Several immune cell subsets demonstrated remarkable stability post-intervention. As depicted in Figure 2a, macrophages did not change significantly following the initial intervention, with the proportion

remaining almost the same, 7.3% in the first intervention and 7.1% in the second intervention (*p*-value = 0.440). Similarly, lymphocytes maintained consistent representation at approximately 14% of total cells with a *p*-value of 0.466. Plasma cells exhibited a trend towards increasing after the weight loss procedure, rising from 1.9% in the first intervention to 2.5% in the second, although this change was not statistically significant (*p*-value = 0.128).

In contrast, neutrophils showed a significant increase in proportion after the intervention, rising from 2.9% to 5.1% of the total cells, with a *p*-value of 6.4×10^{-5}. Notably, this neutrophil expansion occurred independently of the temporal interval between interventions (Supplementary Figure S3), indicating a consistent biological response rather than a time-dependent artifact.

Eosinophils also showed significant proportional increases, rising from 0.3% to 0.5% of total cells, with a *p*-value of 5.3×10^{-4}.

To further validate the observed increase in neutrophils, we performed IHC staining for $CD15^+$ cells in paired liver tissue samples across both timepoints (Figure 2b). $CD15^+$ cells increased from 1.2% to 3.2% (*p*-value = 2.2×10^{-6}), providing independent validation of our findings. Additionally, $CD15^+$ cell proportions demonstrated strong positive correlation with LiverExplore-derived neutrophil abundance ($\rho = 0.68$, *p*-value = 7.2×10^{-12}), supporting the reliability of both analytical approaches and reinforcing the notion that neutrophil recruitment is a prominent feature of the liver's immune adaptation following sleeve gastrectomy.

Beyond quantitative changes, the immune system underwent substantial spatial reorganization following surgery. These alterations extended beyond overall cell abundance to encompass distinct zonal distribution patterns across different hepatic regions. Zones 2 and 3 demonstrated the most pronounced reorganization, with nearly all evaluated immune cell populations exhibiting altered distribution patterns. This comprehensive restructuring indicates a fundamental remodeling of the hepatic immune landscape in response to surgical intervention (Supplementary Figure S4).

These findings reveal a dynamic and multifaceted reorganization of the hepatic immune microenvironment following bariatric surgery. While polymorphonuclear cells, particularly neutrophils and eosinophils, exhibit the most pronounced quantitative increases, the broader immune system demonstrates significant spatial redistribution. This comprehensive immune remodeling suggests that coordinated cellular responses, rather than isolated population changes, drive the liver's adaptive response to surgery-induced metabolic alterations and may be integral to hepatic recovery and repair processes.

4. Dynamic Changes in Hepatic Fibrosis Distribution Post-Surgery

Several distinct subtypes of liver fibrosis exist, each with varying responses to surgical intervention. Periportal fibrosis occurs around the portal tracts, while perisinusoidal fibrosis affects the space of Disse, the area between liver endothelial cells and hepatocytes. Incomplete septal fibrosis is an early

stage of complete septal fibrosis, where fibrotic tissue begins to bridge lobules without forming complete fibrous septa. Complete septal fibrosis signifies advanced scarring, characterized by thick septa of fibrous tissue that disrupts normal liver architecture and can progress to cirrhosis. The most severe form is nodular fibrosis, marked by the formation of regenerative nodules surrounded by fibrous tissue, typically observed in cirrhosis and chronic liver damage[33,34] (Supplementary Figure S5).

Apparent changes in fibrosis are observed following bariatric surgery, as depicted in the upper section of Figure 3. As illustrated in Figure 3b, following steatosis correction, the overall area proportion of pathological fibrosis (defined as the combined periportal, perisinusoidal, incomplete septal, complete septal, and nodular fibrosis subtypes) was not significantly changed (*p*-value = 0.803).

We next assessed the area proportion of individual fibrosis subtypes. Analyzing specific subtypes reveals no significant changes in perisinusoidal fibrosis post-surgery, evidenced by a *p*-value of 0.125. In contrast, periportal fibrosis significantly decreases, dropping from 0.06% to 0.02% of the total tissue area, with a *p*-value of $2.2x10^{-4}$. Similarly, incomplete septal fibrosis also shows a statistically significant decrease, falling from 0.06% to 0.02% (*p*-value = $6.9x10^{-6}$), further supporting the trend of fibrosis reduction post-surgery. Among advanced fibrosis subtypes, complete septal fibrosis shows a marked reduction, decreasing from 0.14% to 0.05% of the total tissue area, with a *p*-value of $6.6x10^{-4}$.Conversely, nodular fibrosis exhibited a non-significant trend toward increase following the intervention. Before surgery, nodular fibrosis accounted for 0.4% of the total tissue area, while after the surgical intervention and subsequent weight loss, this proportion increased to 0.6% (*p*-value = 0.059).

Discussion

Bariatric surgery has demonstrated remarkable efficacy in improving liver health among patients with severe obesity-associated MASH. However, the underlying mechanisms driving hepatic recovery remain poorly understood. Liver biopsy represents the gold standard for evaluating MASH resolution, yet its clinical utility is constrained by significant procedural and analytical limitations. The invasive nature of biopsies, inherent sampling variability, and ethical concerns regarding repeated procedures substantially limit comprehensive longitudinal assessment of hepatic recovery[35–38]. Conventional histological assessments, although valuable, are subjective and prone to intra- and inter-observer variability. These evaluations fail to capture the complex spatial architecture and cellular heterogeneity involved in liver remodeling[39,40]. Such limitations are particularly significant given that the growing global burden of MASH is projected to become the leading cause of liver transplantation by 2030[41–44]. In this regard, AI-enhanced digital pathology may represent a promising tool to maximize diagnostic insights.

We applied LiverExplore, an AI-driven digital pathology tool for the quantitative characterization of liver histology, to a cohort of patients with severe obesity who underwent sequential bariatric procedures. Liver wedge biopsies were obtained during the first and the second interventions. Despite achieving significant BMI reduction, patients remained severely obese. Significant modifications occurred across all assessed parameters of liver health, including improvements in steatosis and ballooning consistent

with results obtained in patients with less extreme obesity[36,45,46], as well as notable changes in fibrosis and immune parameters.

Unlike fibrosis in other organs such as the heart, lungs, or kidneys, hepatic fibrosis has shown remarkable potential for reversibility through mechanisms involving myofibroblast apoptosis, matrix metalloproteinase activation, and collagen degradation[47–49]. This unique regenerative capacity provides important context for interpreting our fibrosis findings. However, fibrosis cannot be quantified using visual examination of conventional H&E staining. LiverExplore, the AI-powered algorithm used in this study, identifies structural and fibrotic collagen present in a digitized H&E-stained whole slide image overlay and quantifies each fibrosis subtype, allowing for accurate and granular assessment of liver fibrosis. Although changes in overall fibrosis were not detected between the first and second interventions in this cohort, we observed meaningful improvements in specific subtypes following LSG. Our AI-enhanced analysis revealed significant decreases in periportal fibrosis, incomplete septal fibrosis, and complete septal fibrosis after surgery.While not statistically significant, a trend toward increased nodular fibrosis was detected at the time of the second intervention. This finding could reflect a true limitation of LSG to reverse severe fibrosis on the timescales observed in this study. Alternatively, as the model was trained to analyze core needle biopsies, it is possible that it has reduced accuracyfor distinguishing nodular fibrosis from structural collagen in the much larger wedge biopsies used in this study. These observed improvements in specific fibrosis subtypes, even in the absence of complete resolution, suggest that bariatric surgery initiates hepatic remodeling processes that may continue to evolve over extended follow-up periods, capitalizing on the liver's inherent capacity for fibrotic tissue remodeling.

A particularly intriguing finding of our study is the post-surgical increase in immune cell infiltration, especially polymorphonuclear cells, which challenges the traditional understanding of liver recovery. While previous research has emphasized inflammation resolution as central to liver improvement[50–53], our data reveals a more nuanced process, with elevated neutrophil and eosinophil levels suggesting active immune-mediated tissue remodeling. The AI-enhanced digital pathology approach used for this study enabled detection of these changes with unprecedented precision, moving beyond traditional pathology's limitation of simply identifying inflammatory foci to characterizing the specific immune cell subtypes and their spatial distribution patterns during post-bariatric liver recovery.

The observed increase in neutrophil levels seems paradoxical given their established role in MASH progression through ROS generation, proteolytic enzyme release, and pro-inflammatory signaling. However, recent evidence points to their context-dependent functions[54]. In the post-bariatric setting, neutrophils appear to transition toward regulatory and reparative roles through several mechanisms: distinct functional subsets may emerge[55], neutrophil-released matrix metalloproteinases contribute to fibrosis remodeling, and microRNA-223 modulates immune responses by promoting anti-inflammatory macrophage polarization[56,57]. Furthermore, the process of efferocytosis, described as macrophage-mediated clearance of apoptotic neutrophils, reinforces this anti-inflammatory shift[58].

The spatial redistribution of immune cells across hepatic tissue could suggest an orchestrated repair process rather than pathological inflammation alone. These findings align with emerging evidence that controlled inflammatory responses may facilitate tissue repair and regeneration[59–61], challenging conventional views about inflammation's role in MASH recovery.

Our study has several limitations. As an exploratory pilot study, our findings require validation in larger and more diverse cohorts. Given the experimental design and ultimate patient population (those who required a second LSG), we cannot claim that the changes we observed are due to weight loss. Additionally, the retrospective study design introduces potential selection bias, while variable time intervals between primary and revisional procedures may confound the interpretation of histological evolution. For ethical considerations, we could not include a matched control group of patients who underwent successful primary LSG without requiring revision surgery, which would have provided valuable comparative data. The absence of standardized timing intervals, while unavoidable in observational research, limits our ability to establish temporal relationships between metabolic recovery and immune system reorganization. Future prospective studies incorporating larger cohorts, standardized follow-up intervals, and longitudinal tissue sampling will be essential to delineate the mechanistic pathways underlying these hepatic immune adaptations and their relationship to bariatric surgery outcomes.

In conclusion, this study demonstrates the transformative potential of AI-enhanced digital pathology in understanding liver disease progression and recovery. By applying this innovative approach to paired liver biopsies from LSG patients, we provided detailed quantitative insights into post-bariatric liver recovery that were previously unattainable through conventional histological assessment. Our findings revealed significant improvements in key liver health parameters and, importantly, uncovered an unexpected yet potentially beneficial role of immune cell infiltration in tissue repair. This novel understanding of immune system dynamics suggests promising therapeutic possibilities through targeted immunomodulation strategies. Furthermore, this study shows how digital pathology can overcome traditional histological limitations by enabling precise quantification and objective assessment of complex tissue changes, opening new avenues for both understanding disease mechanisms and evaluating targeted treatments in MASH and other liver conditions.

Declarations

Funding

This work was supported by Instituto de Salud Carlos III (Madrid Spain) co-funded by the European Union, grant numbers PI18/00921, PI21/00510 and PI24/01146.

Conflicts of Interest:

The authors declare that they have no competing interests.

Financial Support Statement:

Grants from the Instituto de Salud Carlos III (PI18/00921, PI21/00510, PI24/01146) and the European Union co-funded research.

Authors Contributions:

A.-I.O. performed conceptualization, methodology, software, validation, formal analysis, investigation, data curation, writing - original draft, visualization and project administration; L.M., Y.G., G.S., and R.E., provided software and supervision; S.G.-S. provided investigation, software; V.C.-C. and A.J.F., performed investigation, writing - review & editing, software; C.G., provided investigation, resources; D.P., J.C., and J.J., performed supervision, funding acquisition and project administration.

Data Availability:

We are pleased to offer our data to research groups that show interest. Please feel free to reach out to alinaiuliana.onoiu@iispv.cat.

Clinical Trial Number: NCT05554224

References

1. Obesity and overweight. Accessed June 30, 2025. https://www.who.int/news-room/fact-sheets/detail/obesity-and-overweight
2. Craig M Hales MDC. Prevalence of Obesity and Severe Obesity Among Adults: United States, 2017–2018 - PubMed. *NCHS Data Brief*. 2020;360:1–8. Accessed June 30, 2025. https://pubmed.ncbi.nlm.nih.gov/32487284/
3. Santana CVN, Magno LAV, Ramos AV, et al. Genetic Variations in AMPK, FOXO3A, and POMC Increase the Risk of Extreme Obesity. *J Obes*. 2024;2024:3813621. doi:10.1155/2024/3813621
4. Twig G, Reichman B, Afek A, et al. Severe obesity and cardio-metabolic comorbidities: a nationwide study of 2.8 million adolescents. *Int J Obes*. 2019;43(7):1391–1399. doi:10.1038/S41366-018-0213-Z
5. Wong RJ, Aguilar M, Cheung R, et al. Nonalcoholic steatohepatitis is the second leading etiology of liver disease among adults awaiting liver transplantation in the United States. *Gastroenterology*. 2015;148(3):547–555. doi:10.1053/j.gastro.2014.11.039
6. Cabré N, Luciano-Mateo F, Fernández-Arroyo S, et al. Laparoscopic sleeve gastrectomy reverses non-alcoholic fatty liver disease modulating oxidative stress and inflammation. *Metabolism*. 2019;99:81–89. doi:10.1016/j.metabol.2019.07.002
7. Fakhry TK, Mhaskar R, Schwitalla T, Muradova E, Gonzalvo JP, Murr MM. Bariatric surgery improves nonalcoholic fatty liver disease: a contemporary systematic review and meta-analysis. *Surgery for Obesity and Related Diseases*. 2019;15(3):502–511. doi: 10.1016/j.soard.2018.12.002

8. Lassailly G, Caiazzo R, Ntandja-Wandji LC, et al. Bariatric Surgery Provides Long-term Resolution of Nonalcoholic Steatohepatitis and Regression of Fibrosis. *Gastroenterology*. 2020;159(4):1290–1301.e5. doi:10.1053/j.gastro.2020.06.006
9. Chaim FDM, Pascoal LB, Chaim FHM, et al. Histological grading evaluation of non-alcoholic fatty liver disease after bariatric surgery: a retrospective and longitudinal observational cohort study. Sci Rep. 2020;10(1). doi:10.1038/S41598-020-65556-2
10. Kushner RF, Shapiro M. Obesity: assessment and treatment across the care continuum. Ann Med. 2025;57(1):2521433. doi:10.1080/07853890.2025.2521433
11. Ratziu V, Francque S, Behling CA, et al. Artificial intelligence scoring of liver biopsies in a phase II trial of semaglutide in nonalcoholic steatohepatitis. *Hepatology*. 2024;80(1):173–185. doi:10.1097/HEP.0000000000000723
12. FDA Approves Treatment for Serious Liver Disease Known as 'MASH' | FDA. Accessed August 27, 2025. https://www.fda.gov/drugs/news-events-human-drugs/fda-approves-treatment-serious-liver-disease-known-mash
13. Wiebe N, Tonelli M. Long-term clinical outcomes of bariatric surgery in adults with severe obesity: A population-based retrospective cohort study. *PLoS One*. 2024;19(6):e0298402. doi:10.1371/journal.pone.0298402
14. Brown -Chair W, Kow L, Mehran Anvari A, et al. 8 TH GLOBAL REGISTRY REPORT International Federation for Surgery for Obesity and Metabolic Disorders Members of the IFSO Global Registry Committee 1.
15. Głuszyńska P, Łukaszewicz A, Diemieszczyk I, et al. The Effect of Laparoscopic Sleeve Gastrectomy on the Course of Non-Alcoholic Fatty Liver Disease in Morbidly Obese Patients during One Year of Follow Up. *J Clin Med*. 2023;12(12). doi:10.3390/JCM12124122
16. Esquivel CM, Garcia M, Armando L, Ortiz G, Lascano FM, Foscarini JM. Laparoscopic Sleeve Gastrectomy Resolves NAFLD: Another Formal Indication for Bariatric Surgery? *Obes Surg*. 2018;28(12):4022–4033. doi:10.1007/S11695-018-3466-7
17. Huttasch M, Roden M, Kahl S. Obesity and MASLD: Is weight loss the (only) key to treat metabolic liver disease? *Metabolism*. 2024;157. doi:10.1016/j.metabol.2024.155937
18. Harrison SA, Bedossa P, Guy CD, et al. A Phase 3, Randomized, Controlled Trial of Resmetirom in NASH with Liver Fibrosis. *New England Journal of Medicine*. 2024;390(6):497–509. doi:10.1056/NEJMOA2309000
19. FDA Approves Treatment for Serious Liver Disease Known as 'MASH' | FDA. Accessed November 20, 2025. https://www.fda.gov/drugs/news-events-human-drugs/fda-approves-treatment-serious-liver-disease-known-mash
20. Kleiner DE, Brunt EM, Van Natta M, et al. Design and validation of a histological scoring system for nonalcoholic fatty liver disease. *Hepatology*. 2005;41(6):1313–1321. doi:10.1002/HEP.20701
21. Harrison SA, Dubourg J. Liver biopsy evaluation in MASH drug development: Think thrice, act wise including those for text and data mining, AI training, and similar technologies. *J Hepatol*.

2024;81:886–894. doi:10.1016/j.jhep.2024.06.008

22. Sanyal P, Biswas D, Mitra S. Artificial Intelligence in Liver Pathology: Precision Histology for Accurate Diagnoses. J Clin Exp Hepatol. 2025;15(6):103145. doi:10.1016/J.JCEH.2025.103145
23. Neuschwander-Tetri BA, Akbary K, Carpenter DH, Noureddin M, Alkhouri N. The emerging role of second harmonic generation/two photon excitation for precision digital analysis of liver fibrosis in MASH clinical trials. J Hepatol. 2025;83(3):790–799. doi:10.1016/j.jhep.2025.04.026
24. Taylor-Weiner A, Pokkalla H, Han L, et al. A Machine Learning Approach Enables Quantitative Measurement of Liver Histology and Disease Monitoring in NASH. *Hepatology*. 2021;74(1):133–147. doi:10.1002/HEP.31750
25. Grignaffini F, Barbuto F, Troiano M, et al. The Use of Artificial Intelligence in the Liver Histopathology Field: A Systematic Review. *Diagnostics*. 2024;14(4). doi:10.3390/DIAGNOSTICS14040388
26. Iyer JS, Juyal D, Le Q, et al. AI-based automation of enrollment criteria and endpoint assessment in clinical trials in liver diseases. *Nat Med*. 2024;30(10):2914–2923. doi:10.1038/S41591-024-03172-7
27. Pulaski H, Harrison SA, Mehta SS, et al. Clinical validation of an AI-based pathology tool for scoring of metabolic dysfunction-associated steatohepatitis. Nature Medicine 2024 31:1. 2024;31(1):315–322. doi:10.1038/s41591-024-03301-2
28. Łabul M, Wysocki M, Małczak P, et al. The outcomes of Re-Redo bariatric surgery—results from multicenter Polish Revision Obesity Surgery Study (PROSS). *Sci Rep*. 2024;14(1):1–9. doi:10.1038/S41598-024-52817-7
29. Neuberger J, Patel J, Caldwell H, et al. Guidelines on the use of liver biopsy in clinical practice from the British Society of Gastroenterology, the Royal College of Radiologists and the Royal College of Pathology. *Gut*. 2020;69(8):1382–1403. doi:10.1136/gutjnl-2020-321299
30. Stanford-Moore A, Patel N, Gerardin Y, et al. Comprehensive characterization of granular fibrotic and cellular features in liver tissue enabled by deep learning models. *medRxiv*. Published online June 30, 2025:2025.06.12.25328580. doi:10.1101/2025.06.12.25328580
31. Diao JA, Wang JK, Chui WF, et al. Human-interpretable image features derived from densely mapped cancer pathology slides predict diverse molecular phenotypes. Nature Communications 2021 12:1. 2021;12(1):1–15. doi:10.1038/s41467-021-21896-9
32. Sergi CM. NAFLD (MASLD)/NASH (MASH): Does It Bother to Label at All? A Comprehensive Narrative Review. Int J Mol Sci. 2024;25(15). doi:10.3390/IJMS25158462
33. Pais R, Aron-Wisnewsky J, Bedossa P, et al. Persistence of severe liver fibrosis despite substantial weight loss with bariatric surgery. *Hepatology*. 2022;76(2):456–468. doi:10.1002/HEP.32358
34. Schinoni MI, Andrade Z, de Freitas LAR, Oliveira R, Paraná R. Incomplete septal cirrhosis: an enigmatic disease. *Liver International*. 2004;24(5):452–456. doi:10.1111/J.1478-3231.2004.0989.X
35. Lassailly G, Caiazzo R, Ntandja-Wandji LC, et al. Bariatric Surgery Provides Long-term Resolution of Nonalcoholic Steatohepatitis and Regression of Fibrosis. *Gastroenterology*. 2020;159(4):1290–1301.e5. doi:10.1053/j.gastro.2020.06.006

36. Lassailly G, Caiazzo R, Goemans A, et al. Resolution of Metabolic Dysfunction-associated Steatohepatitis With No Worsening of Fibrosis After Bariatric Surgery Improves 15-year Survival: A Prospective Cohort Study. *Clinical Gastroenterology and Hepatology*. Published online 2025. doi:10.1016/j.cgh.2024.10.025
37. Longerich T, Schirmacher P. Determining the reliability of liver biopsies in NASH clinical studies. *Nat Rev Gastroenterol Hepatol*. 2020;17(11):653–654. doi:10.1038/S41575-020-00363-8
38. Sumida Y, Nakajima A, Itoh Y. Limitations of liver biopsy and non-invasive diagnostic tests for the diagnosis of nonalcoholic fatty liver disease/nonalcoholic steatohepatitis. *World J Gastroenterol*. 2014;20(2):475–485. doi:10.3748/WJG.V20.I2.475
39. Onoiu AI, Domínguez DP, Joven J. Digital Pathology Tailored for Assessment of Liver Biopsies. *Biomedicines 2025, Vol 13, Page 846*. 2025;13(4):846. doi: 10.3390/biomedicines13040846
40. Taylor-Weiner A, Pokkalla H, Han L, et al. A Machine Learning Approach Enables Quantitative Measurement of Liver Histology and Disease Monitoring in NASH. *Hepatology*. 2021;74(1):133–147. doi:10.1002/HEP.3175
41. Younossi ZM, Marchesini G, Pinto-Cortez H, Petta S. Epidemiology of Nonalcoholic Fatty Liver Disease and Nonalcoholic Steatohepatitis: Implications for Liver Transplantation. Transplantation. 2019;103(1):22–27. doi:10.1097/TP.0000000000002484
42. Younossi Z, Anstee QM, Marietti M, et al. Global burden of NAFLD and NASH: Trends, predictions, risk factors and prevention. *Nat Rev Gastroenterol Hepatol*. 2018;15(1):11–20. doi:10.1038/NRGASTRO.2017.109
43. Huang DQ, El-Serag HB, Loomba R. Global epidemiology of NAFLD-related HCC: trends, predictions, risk factors and prevention. *Nat Rev Gastroenterol Hepatol*. 2021;18(4):223–238. doi:10.1038/S41575-020-00381-6
44. Le P, Tatar M, Dasarathy S, et al. Estimated Burden of Metabolic Dysfunction-Associated Steatotic Liver Disease in US Adults, 2020 to 2050. *JAMA Netw Open*. 2025;8(1):e2454707. doi:10.1001/JAMANETWORKOPEN.2024.54707,
45. Tasabehji D, Saleh S, Mokadem M. Impact of Bariatric Surgery and Endoscopic Therapies on Liver Health in Metabolic Dysfunction-Associated Steatotic Liver Disease: A Review. J Clin Med. 2025;14(12):4012. doi:10.3390/JCM14124012
46. Liu H, Lefere S, Guillot A, Zheng MH, Tacke F. Bariatric surgery for metabolic dysfunction-associated steatotic liver disease (MASLD): Current knowledge of mechanisms. *Hepatology*. Published online 2025. doi:10.1097/HEP.0000000000001417,
47. Ruiz-Blázquez P, Fernández-Fernández M, Pistorio V, et al. Cathepsin D is essential for the degradomic shift of macrophages required to resolve liver fibrosis. *Mol Metab*. 2024;87. doi:10.1016/j.molmet.2024.101989
48. Pei Q, Yi Q, Tang L. Liver Fibrosis Resolution: From Molecular Mechanisms to Therapeutic Opportunities. Int J Mol Sci. 2023;24(11). doi:10.3390/IJMS24119671

49. Sun M, Kisseleva T. Reversibility of Liver Fibrosis. *Clin Res Hepatol Gastroenterol*. 2015;39(01):S60. doi:10.1016/J.CLINRE.2015.06.015
50. He Y, Chen Y, Qian S, et al. Immunopathogenic mechanisms and immunoregulatory therapies in MASLD. Cellular & Molecular Immunology 2025. Published online June 10, 2025:1–19. doi:10.1038/s41423-025-01307-5
51. Tasabehji D, Saleh S, Mokadem M. Impact of Bariatric Surgery and Endoscopic Therapies on Liver Health in Metabolic Dysfunction-Associated Steatotic Liver Disease: A Review. J Clin Med. 2025;14(12):4012. doi:10.3390/JCM14124012
52. Liu H, Lefere S, Guillot A, Zheng MH, Tacke F. Bariatric surgery for metabolic dysfunction-associated steatotic liver disease (MASLD): Current knowledge of mechanisms. *Hepatology*. Published online 2025. doi:10.1097/HEP.0000000000001417,
53. Sawada K, Chung H, Softic S, Moreno-Fernandez ME, Divanovic S. The bidirectional immune crosstalk in metabolic dysfunction-associated steatotic liver disease. *Cell Metab*. 2023;35(11):1852–1871. doi:10.1016/j.cmet.2023.10.009
54. Shim HB, Deniset JF, Kubes P. Neutrophils in homeostasis and tissue repair. *Int Immunol*. 2022;34(8):399–407. doi:10.1093/INTIMM/DXAC029
55. Scapini P, Marini O, Tecchio C, Cassatella MA. Human neutrophils in the saga of cellular heterogeneity: insights and open questions. *Immunol Rev*. 2016;273(1):48–60. doi:10.1111/IMR.12448
56. Houshmandfar S, Saeedi-Boroujeni A, Rashno M, Khodadadi A, Mahmoudian-Sani MR. miRNA-223 as a regulator of inflammation and NLRP3 inflammasome, the main fragments in the puzzle of immunopathogenesis of different inflammatory diseases and COVID-19. *Naunyn Schmiedebergs Arch Pharmacol*. 2021;394(11):2187–2195. doi:10.1007/S00210-021-02163-6
57. Yan L, Wang J, Cai X, et al. Macrophage plasticity: signaling pathways, tissue repair, and regeneration. *MedComm (Beijing)*. 2024;5(8). doi:10.1002/MCO2.658,
58. Elliott MR, Koster KM, Murphy PS. Efferocytosis Signaling in the Regulation of Macrophage Inflammatory Responses. The Journal of Immunology. 2017;198(4):1387–1394. doi:10.4049/JIMMUNOL.1601520
59. Laurent P, Jolivel V, Manicki P, et al. Immune-mediated repair: A matter of plasticity. *Front Immunol*. 2017;8(APR). doi:10.3389/FIMMU.2017.00454,
60. Phillipson M, Kubes P. The Healing Power of Neutrophils. Trends Immunol. 2019;40(7):635–647. doi:10.1016/j.it.2019.05.001
61. Koda Y, Nakamoto N, Kanai T. Regulation of Progression and Resolution of Liver Fibrosis by Immune Cells. Semin Liver Dis. 2022;42(4):475–488. doi:10.1055/A-1957-6384/ID/JR2200047-21/BIB

Figures

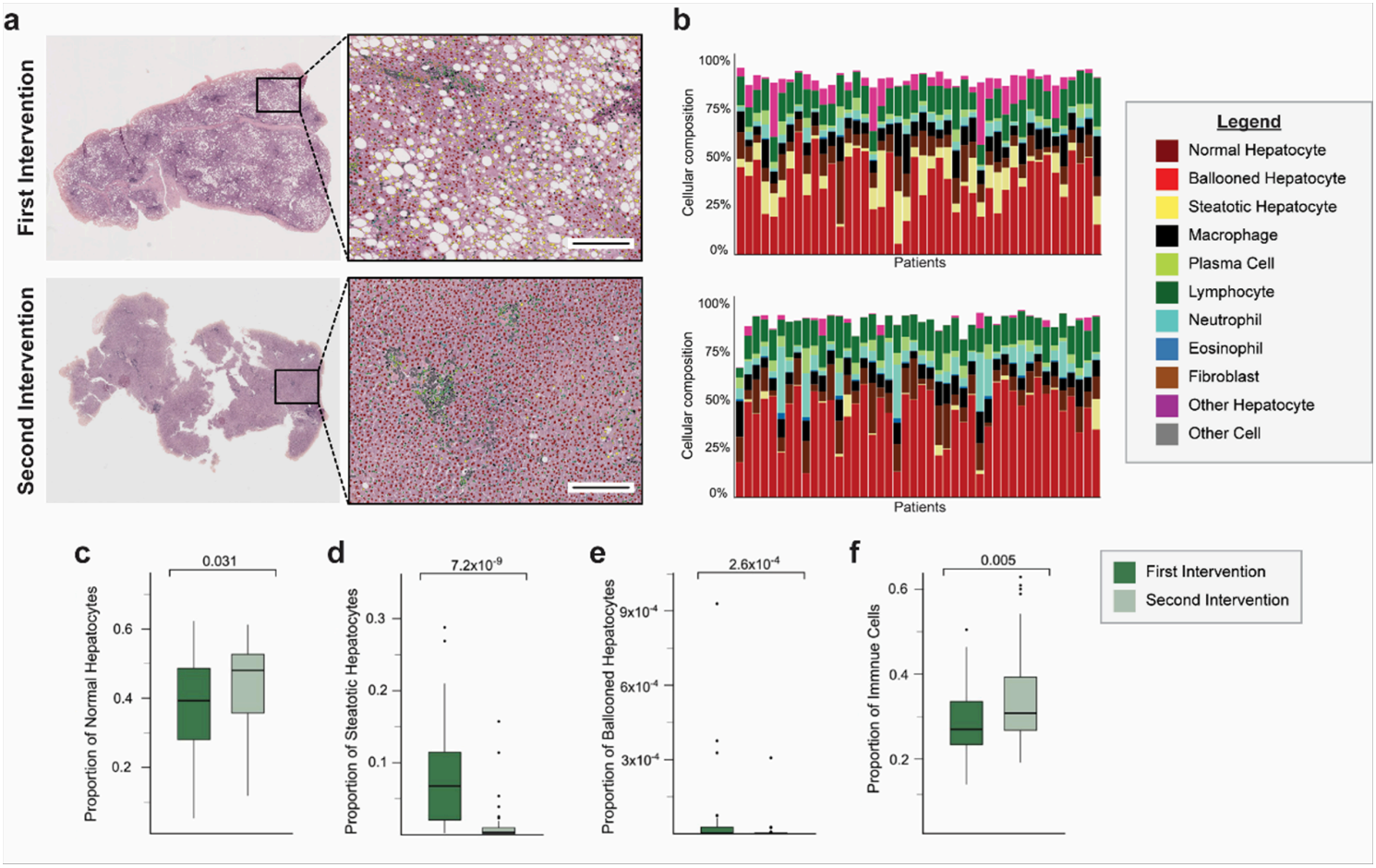


Figure 1

Percentage distribution of different cell types in the liver in the first and the second intervention. (a) *Representative H&E-stained liver biopsies (first and second intervention) from a single patient. Liver Explore cell overlays are included in the high-magnification images. Scale bar: 200 µm.* ***(b)*** *Composition within each patient sample of 9 major cell types. The remaining percentage of the evaluated tissue, accounting for the balance up to 100%, was classified as "other cells". Box plots for normal hepatocytes* ***(c)****, steatotic hepatocytes* ***(d)****, ballooned hepatocytes* ***(e)****, and immune cells* ***(f)****. Immune cells consist of macrophages, eosinophils, neutrophils, plasma cells, and lymphocytes.*

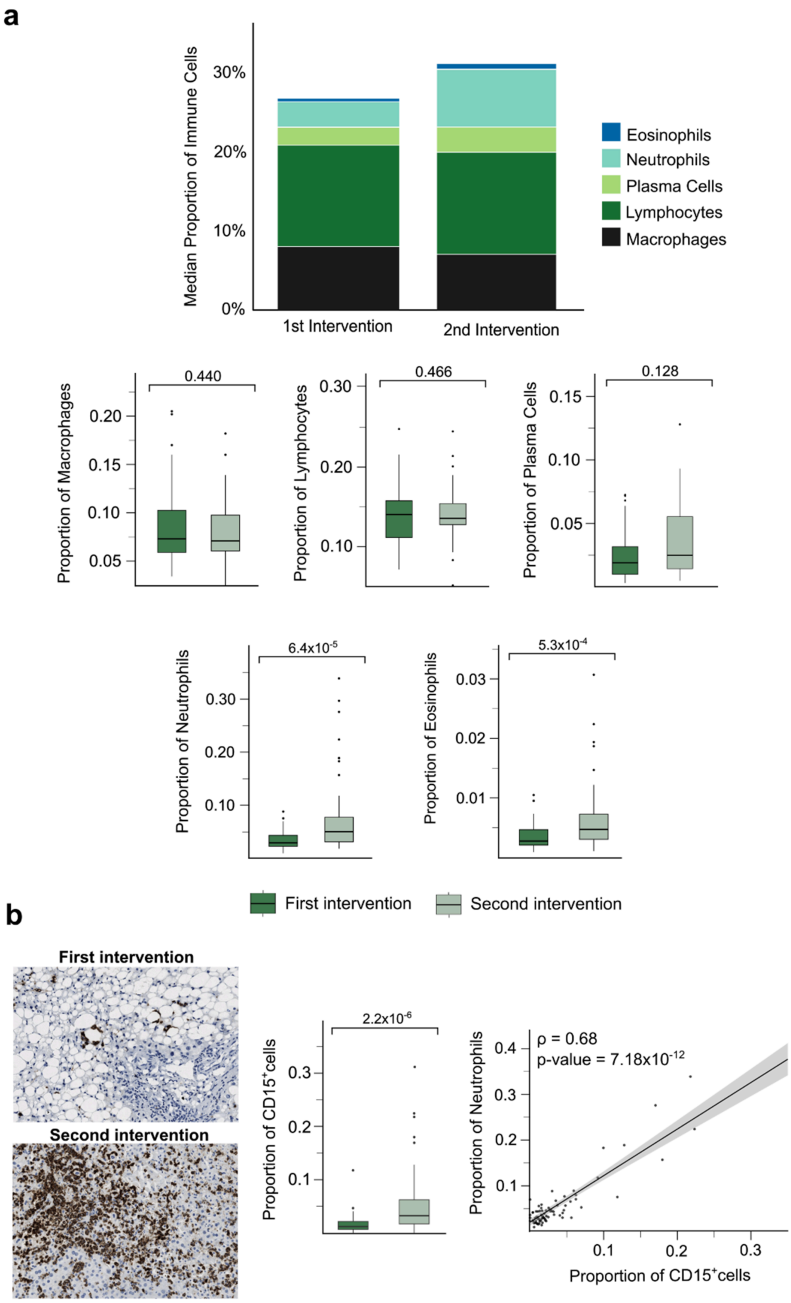


Figure 2

Immune reshaping after surgery highlights the role of neutrophils and eosinophils in liver recovery. (a) *The immune cell population significantly increased after the first intervention, with a notable rise in neutrophils and eosinophils.* ***(b)*** *Representative IHC images (10x magnification) showing CD15^{+} cells before and after surgery. A strong correlation was observed between CD15^{+} cell abundance and neutrophil levels detected by the LiverExplore algorithm.*

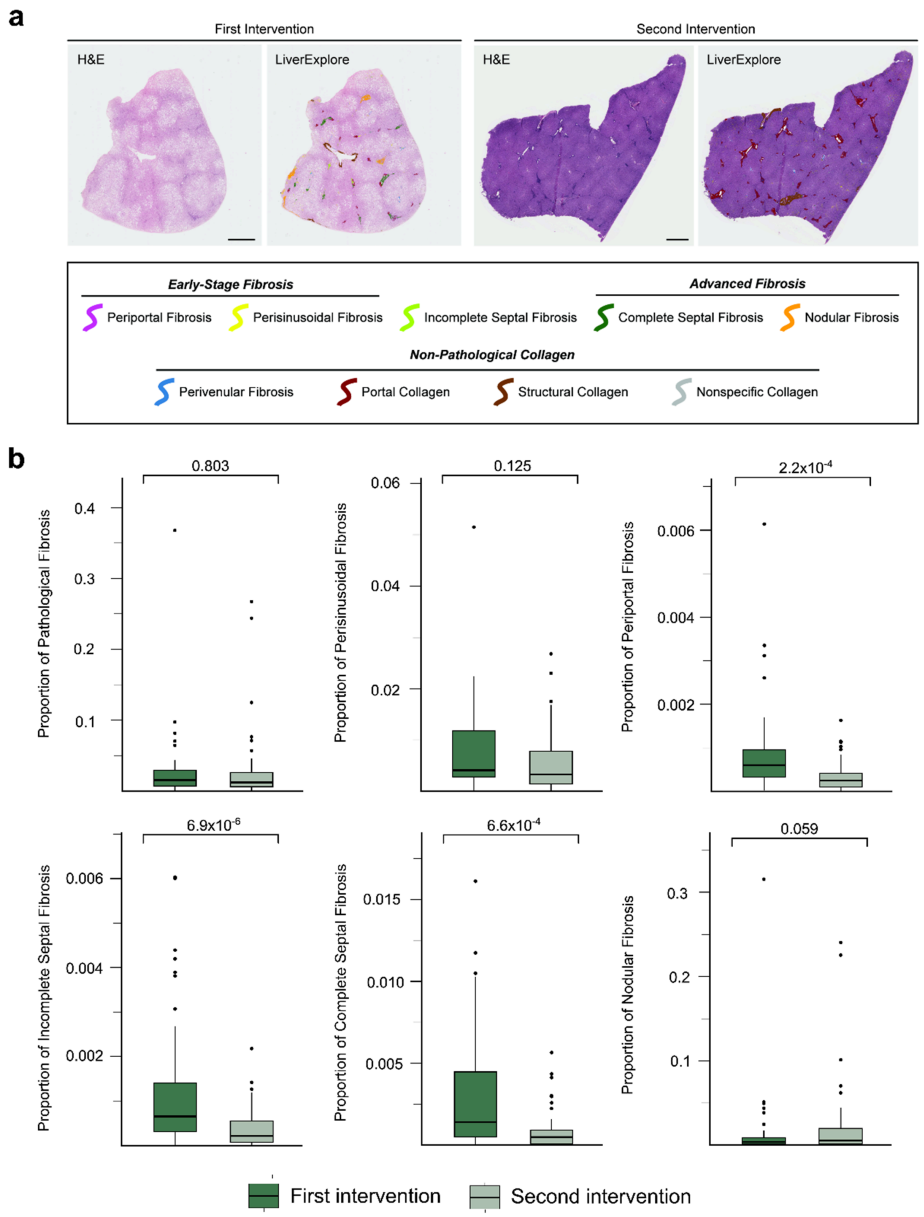


Figure 3

Characterization of hepatic fibrosis changes after bariatric surgery. (a) *Representative whole-slide liver images at 2x magnification stained with H&E and fibrosis segmentation derived from LiverExplore illustrate architectural and fibrotic changes between the first and second interventions.* ***(b)*** *Boxplots display the quantified proportions of different fibrotic structures.*

Supplementary Files

This is a list of supplementary files associated with this preprint. Click to download.

- Supplementarymat.docx